Carbonates and Evaporites (2019) 34:1669–1687
https://doi.org/10.1007/s13146-019-00515-1

ORIGINAL ARTICLE

Reef-carbonate diagenesis in the Pleistocene–Holocene of the well Xike#1, Xisha Islands, South China Sea: implications on sea-level changes

Na Liu[1] · Zhen-feng Wang[2] · Xu-shen Li[2] · Li Liu[1] · Dao-jun Zhang[2] · Li You[2] · Wei Luo[2] · Xin-yu Liu[2]

Accepted: 2 July 2019 / Published online: 15 July 2019

Abstract

The Pleistocene was characterized by an unstable meteoric–marine diagenetic environment, influenced by high-amplitude global and regional eustatic variations. This paper focuses on the diagenetic characteristics of the Pleistocene–Holocene reef-carbonate rocks in the well Xike#1, drilled on the Stone Island (part of the Xisha Islands) in the South China Sea. A petrographic, cathodoluminescence and stable isotope study allowed the evaluation of the diagenetic evolution of the reef-carbonate rocks. The rock types present include framestones, packstones, wackestones and grainstones. Rock fabric analysis reveals the existence of skeletal grains, biodetritus, intraclasts, matrix and calcite cements. The upper part of the cored interval (0–180 m) has been heavily altered by meteoric fluids. Unequivocal evidence of meteoric diagenesis includes consistently negative $\delta^{18}O$ values, well-developed subaerial exposure horizons and typical vadose cements. The deepest exposure surface is ~ 80 m above the base of meteoric diagenesis, which means that the paleowater table could be extended to as deep as 80 m. The grainstone present at 7.74 m represents the boundary between the vadose and phreatic zones, which is marked by the first appearance of isopachous dogtooth cements and well-developed moldic pores. The reef-carbonate rocks between depths of 21.66 m and 180 m have undergone diagenesis in both meteoric and marine environments, in which the early-stage fibrous marine cements are surrounded by later meteoric drusy calcite cements. The end products of phreatic meteoric diagenesis are the limestones composed of low-Mg calcite with micrite envelopes, moldic pores, blocky spar calcite cementation, and aragonite neomorphism. The interval from 180 to 216 m has undergone a marine diagenesis, which is marked by cements with non-luminescent CL characteristic and a limited, relatively enriched C and O isotope composition. The study reveals that the diagenetic evolution of reef carbonate is mainly controlled by high-frequency eustatic sea-level changes, while the sedimentation rate variations, which were induced by regional subsidence and nutrient variations could also have had an impact on the diagenetic evolution.

Keywords Reef carbonate · Diagenetic evolution · Pleistocene–Holocene · Xisha Islands

Introduction

Carbonate diagenesis in shallow marine environments has been well studied in recent decades, as the diagenetic products have had a major impact on the macroscopic, microscopic and petrophysical properties of sedimentary successions (e.g., Allan and Matthews 1982; Budd and Land 1990; Quinn 1991; Liu et al. 1997). Reef carbonates are the key recorder of both sea level and associated environmental changes. They can provide reliable geological estimates of past relative sea level and paleoenvironment (Quade and Roe 1999; Benito and Mas 2006; Fox et al. 2012; Singh et al. 2012; Solihuddin et al. 2015; Shao et al. 2017), i.e., most of the history of Pleistocene–Holocene sea-level changes, are stored on modern fore-reef slopes in relatively stable tectonic settings. The last ca 800 kyr have been typified by rapid sea-level changes (e.g., Waelbroeck et al. 2002; Lambeck et al. 2002). The atolls (ring-shaped coral reef islands) thus commonly experience repeated emergence and flooding due to regular eustasy. Therefore, atolls are seen as favorable

✉ Li Liu
liuli0892@vip.sina.com

[1] College of Earth Sciences, Jilin University, 2199 Jianshe Street, Changchun 130061, Jilin, China

[2] China National Offshore Oil Corporation Limited, Zhanjiang 524057, Guangdong, China

localities for investigating the diagenesis of carbonates in both freshwater and marine environments (e.g., Lincoln and Schlanger 1987; Quinn 1991; Kindler and Mazzolini 2001; Kumar et al. 2012; Yasukochi et al. 2014).

Studies on the diagenesis of reef carbonates have generally involved descriptions of their fabric, mineralogy and geochemical characteristics with respect to changes in sea level (e.g., Allan and Matthews 1977; Buchbinder and Friedman 1980; Saller and Moore 1989; Follows 1992; Vollbrecht and Meischner 1996; Li and Jones 2013a, b; Woodroffe and Webster 2014). The whole-rock mineralogy and geochemistry investigation have been proven to be effective in distinguishing between meteoric and marine diagenesis in carbonate successions (e.g., Major and Matthews 1983; Melim et al. 2004; Gischler et al. 2013).

The Xisha Islands, located in the South China Sea (SCS), include many atolls and therefore offer an excellent opportunity to study the diagenetic evolution of carbonates. A series of scientific and commercial drilling programs have been conducted on the Xisha Islands in the 1970s and 1980s and provided data on the biostratigraphy, lithology, sedimentology, paleomagnetism (e.g., He and Zhang 1990; Zhang 1990; Ye et al. 1991; Liu et al. 1997). However, these previous studies of the Xisha carbonate platforms were limited to shallow drill holes and field surveys of surface geology. A brand-new scientific borehole, Xike#1, with the core recovery rate as high as 80%, was drilled on the Stone Island of Xisha Islands during 2013–2014. This cored interval is the researching target in this paper.

Several authors have contributed to the regional geology, tectonic development, fossil components, elemental geochemistry and the carbonate platform evolution of the Xisha Islands (e.g., Wu et al. 2014; Qiao et al. 2015; Zhai et al. 2015; Zhu et al. 2016; Shao et al. 2017; Wang et al. 2018; Ma et al. 2018). Recently, Wu et al. (2019) studied the evolution of the reef-bank system since the Pliocene based on the sedimentological, paleontological and geochemical data. However, the above-mentioned studies did not tie diagenesis analysis and the diagenetic evolution. During the Pleistocene glacioeustatic sea-level fluctuations, the alternation of meteoric diagenesis and marine diagenesis has been considered the greatest factor in the diagenesis of the Pleistocene–Holocene shallow-water carbonates. The geometry, composition and evolution of the diagenetic products are the direct key recorders of these changes. It is therefore important to have a good understanding of the diagenetic history of the reef material.

In this paper, we document the diagenetic evolution history of the reef-carbonate rocks in the Pleistocene–Holocene of Xike#1 on the Xisha Islands. The interpretations of meteoric and marine diagenesis are discussed, respectively, through a petrographic, cathodoluminescence and geochemical study. An attempt was carried out to describe the diagenetic evolution history since the Pleistocene and to judge the impact of sea-level changes on the diagenetic evolution. Our results show that besides the high-frequency eustatic sea-level changes, the sedimentation rate variations induced by regional subsidence and nutrient variations also have an impact on diagenetic evolution.

Geological setting

The Xisha Islands (15°15′–17°0′N, 111°–113°E), that developed on the Xisha Uplift in the northwest of the South China Sea, consist of more than 40 islands, sandbanks and reefs. These islands are divided into two groups: the eastern Xuande archipelago and the western Yongle archipelago (Shao et al. 2017). Xuande archipelago consists of approximately 11 small islands surrounding a lagoon 40 km long by 20 km wide with a maximum depth of 67 m, whereas Yongle archipelago consists of approximately 7 small islands surrounding a lagoon 20 km long by 15 km wide with a maximum depth of 45 m. The Xisha Uplift had experienced rifting since the late Cretaceous, and gradually drifted southwards from the South China continent during the late Eocene and early Oligocene, and then subsided during the late Oligocene to early Miocene period of seafloor spreading (Wu et al. 2014, 2019).

Since the early Miocene, multiple reefs have been well developed in the Xisha archipelago (Ma et al. 2018), which were mainly shaped by geotectonics, global eustasy and climatic variation (Wu et al. 2014). During the last glacial period, Xisha Islands experienced a subtropical climate with surface water temperatures that were 18.1–23.8 °C (Huang et al. 1997; Pelejero et al. 1999; Chen et al. 2005). Today, the mean annual temperature in Xisha islands ranges from 22.9 to 34.4 °C, with a yearly average rainfall of 130 ~ 200 cm/year and annual evaporation averages 150 ~ 250 cm/year (Ye et al. 1987; Zhang et al. 1989).

Stone Island (16°46′N, 112°21′E), which belongs to Xuande archipelago and has an area of only 0.08 km^2, is connected to Yongxing Island by land reclamation. This island has the highest elevation of the Xisha Islands and is the only island that contains lithified carbonate aeolianites. Most of the other islands in this group are covered by piles of reef sediment, mainly coral and shell fragments.

The well Xike#1 was drilled on Stone Island (Fig. 1b) during 2013–2014, with a continuously cored interval to a depth of 1268.2 m (the whole thick carbonate succession is 0–1257.52 m) and a core recovery rate as high as 80%.

Before the well Xike#1, four continuously cored wells have been drilled on the Xisha Islands: Xiyong#1 (drilled on Yongxing Island in 1974, core recovery rate is less than 10%), Xiyong#2 (drilled on Yongxing Island in 1983), Xichen#1 (drilled on Chenhang Island in 1983) and Xishi#1

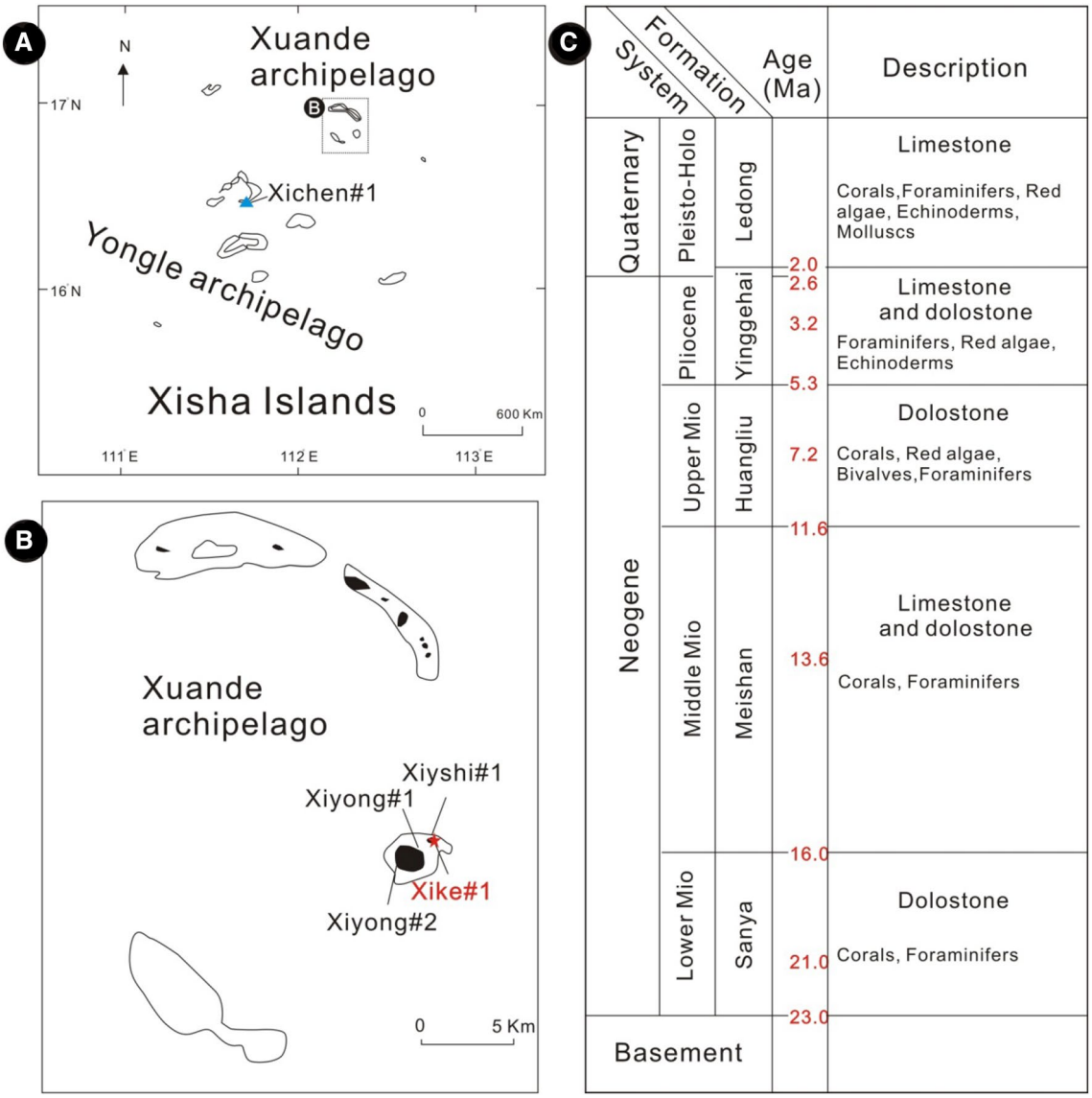

Fig. 1 **a**, **b** Locations of the Xike#1 and previous boreholes drilled in the Xisha Islands. **a** Xisha Islands are divided into two groups: the Xuande archipelago and the Yongle archipelago; **b** locations of Xuande archipelago with positions of wells. **c** Integrated stratigraphic succession of Neogene rocks on the Xisha Islands showing distribution of limestones and dolostones (adapted from Wu et al. 2014; Zhai et al. 2015)

(drilled on Stone Island in 1983). However, these early boreholes were limited in their utility due to an incomplete core recovery and a lack of basement drilling. The identification of fossil components, analyzation on facies and diagenesis has been carried out on the reef successions in these four wells (e.g., Zhang et al. 1989; Zhang 1990; Ye et al. 1991; Liu et al. 1997).

Based on the combination of paleomagnetism, calcareous nanofossils, and planktonic foraminifera, the thick carbonate succession in the well XiKe#1 is divided into five units, including early Miocene interval (Sanya Formation), middle Miocene interval (Meishan Formation), late Miocene interval (Huangliu Formation), Pliocene interval (Yinggehai Formation), and Pleistocene–Holocene interval (Ledong Formation) (Wu et al. 2014; Zhai et al. 2015) (Fig. 1c). Lithological observations show that the reef carbonate dominates in the Pleistocene–Holocene interval (0–216 m).

Materials and methods

All samples used in this study come from the well Xike#1. Fauna identification was attempted in hand specimens, although most of the useful information came from thin

section analysis. A total of 650 thin sections (27 × 46 mm or 51 × 76 mm) were prepared from the core samples, representing approximately 3 thin sections per meter of the core. All of the sections had been impregnated with blue epoxy. Arizarin Red S stain was used on 80 sections to discriminate among various carbonate minerals. The categories of the allochems (including skeletal grains, biodetritus, micrite and cements) were quantified by point counting in thin sections (300 points per section) for identification of the sedimentary fabrics under the Olympus petrographic microscope. Samples were classified using the Dunham carbonate classification scheme (Dunham 1962) and Embry and Klovan's expansion (Embry and Klovan 1971) to include the autochthonous boundstone category (as used by Martindale et al. 2012). Diagenetic mineral textures and morphologies for 12 samples were examined at the RCPS Jilin University using a JSM6700F electron microscope made by the JEOL Company of Japan. 35 samples were studied under the CL, using the CL8200&MK4 instrument made by Cambridge Image Technology Ltd., England.

Carbon (C) and oxygen (O) stable isotope ratios were measured in 45 representative reef-carbonate samples (with powdered bulk samples) using MAT 251 and MAT 253 mass spectrometers at the Institute of Geology Chinese Academy of Geological Sciences and the CNNC Beijing Research Institute of Uranium Geology in China, respectively. The powdered samples were reacted with 100% orthophosphoric acid at 25 °C for 6 h to extract CO_2 for C and O analyses (McCrea 1950). $^{13}C/^{12}C$ and $^{18}O/^{16}O$ ratios are expressed in delta notation ($\delta^{13}C$ and $\delta^{18}O$, respectively) in per mil (‰) relative to the VPDB (Vienna Pee Dee Belemnite) standard. Average internal analytical precision was 0.05‰ and 0.03‰ for $\delta^{13}C$ and $\delta^{18}O$, respectively.

The ages of important surfaces in this paper were established by the linear interpolation between the well-tested age data (Wang et al. 2017; Wu et al. 2019).

Results

Rock fabrics and rock types

The analysis of reef-carbonate rock fabrics revealed skeletal grains, intraclasts, matrix and calcite cements.

Types of grains

Carbonate allochems present include skeletal grains and rare intraclasts. The distribution of different grain types is given in Fig. 2. Coral (deominated by *Turbinaria*, *Favia* and *Cyphastrea*) and red algae, as the main reef-building organisms, are well represented, especially between 21.66 and 94.26 m. Within the biodetritus, foraminifera are abundant, accompanied by some green algae, echinoderms, molluscs and bryozoans. The intraclasts are rare, and present in wacke- and packstone.

Types of carbonate deposits

The types of carbonate deposits are shown in Fig. 3.

Unconsolidated carbonate sands

Carbonate sands are present at 0–2.92 m and 10.88–21.66 m. The deposits consist mostly of medium to coarse grained (particle size: 0.2–1.0 mm), moderately to well-sorted carbonate fragments (Fig. 3a, b) which locally contain benthic foraminifera, calcareous algae, echinoderms and mollusc shells. The deposits that occurred in the uppermost 21 m interval of Xike#1 have been identified as aeolianite facies (Ye et al. 1990; Li et al. 2018; Wu et al. 2019).

Grainstones

Grainstone occurs between carbonate sand layers, and consists mainly of sub-rounded to elongate fragments of red algae and foraminifera (Fig. 3c), with rare molluscs and echinoderms. Calcite cements, which make up ≤ 8% of the rock, consist of small (5–10 μm) meniscus, equigranular, rhombic crystals that are usually found at grain contacts (Fig. 4a, c, g and h), or as isolated isopachous fringes, partially or entirely covering grains (Fig. 4b). Pendant calcite cement is also detected in some samples (Fig. 4d).

Framestones

The framework of the reef is supported by corals and crusts of red algae, which contribute up to 80% of all sedimentary components (Fig. 3d). The corals are dominated by *Turbinaria, Favia* and *Cyphastera,* while the red algal are characterized by *Porites.* Other bioclasts include some foraminifera, rare echinoderms, molluscs and bryozoans. The intra-skeletal porosity is either preserved, or filled with fine-grained bioclastic fragments. Pore-filling fibrous and drusy calcite spar cements are also observed (Fig. 5c and d). The framestones mainly developed in coral reef facies and coral–algal reef facies (Wu et al. 2019).

Packstones

The packstone contains grains made up of angular to sub-rounded fragments of calcareous algae, coralline crusts, foraminifera, molluscs and bryozoans, with most particle sizes in the range of 0.2–1.2 mm. Some grains that have retained their morphological integrity reach greater sizes of 1.5–2.0 mm. The grains make up 60–85% of the whole

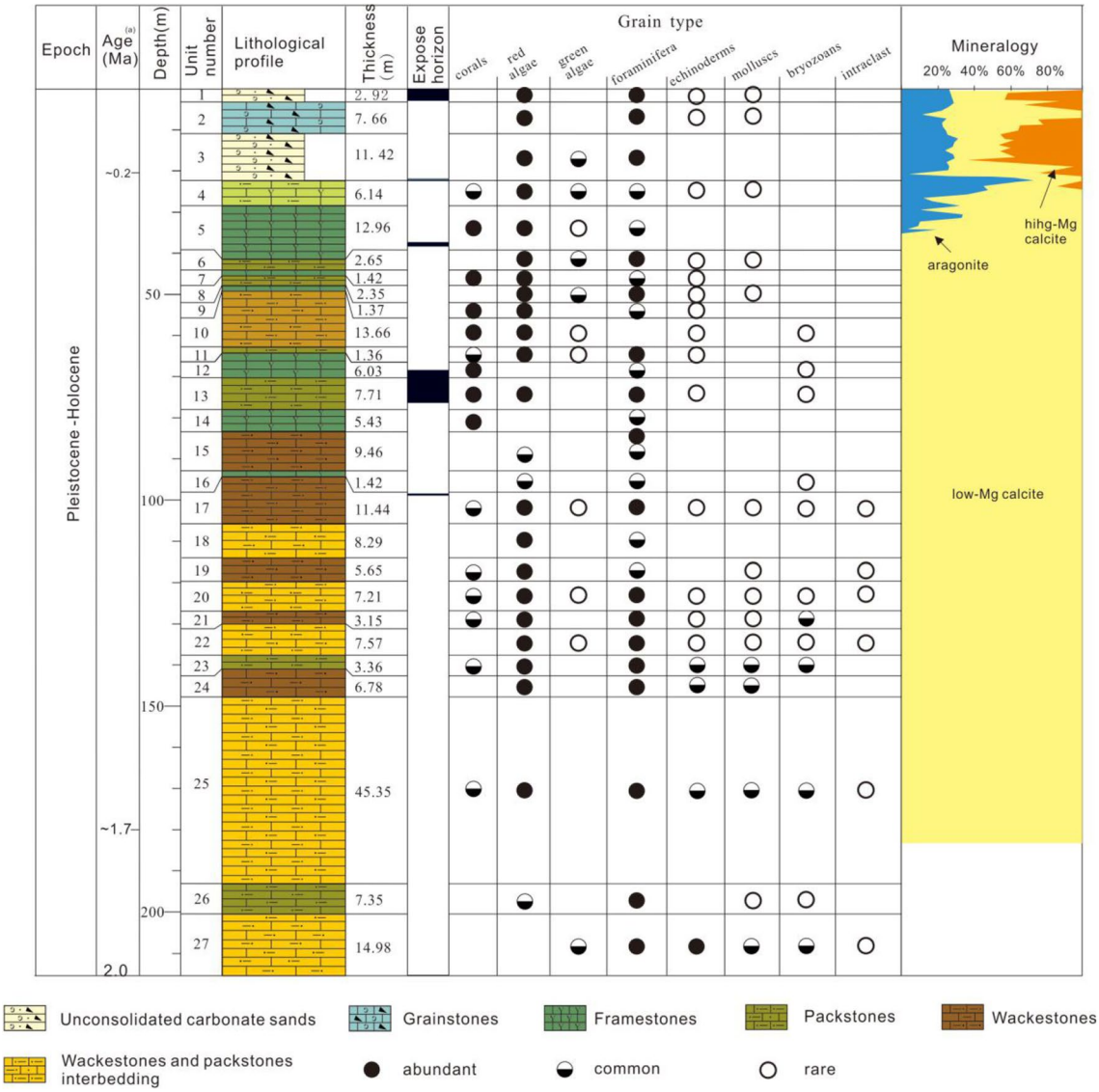

Fig. 2 Lithostratigraphy of Xike#1 in the Pleistocene–Holocene, showing the distribution of the grain types with depth. (1) The ages were established by the linear interpolation between the well-tested age data (Wang et al. 2017; Wu et al. 2019); (2) depth; (3) unit number; (4) lithological profile; (5) thickness; (6) expose horizons; (7) grains types including corals, red algae, green algae, foraminifera, echinoderms, molluscs, bryozoans, intraclast; (8) mineralogy data, which is from Zhai et al. (2015) by XRD analysis, the percentage of aragonite is shown from left to right and percent of high-Mg calcite is from right to left

rock. The matrix (~ 10%–35% of the rock) consists of fine micrite and microspar (Fig. 3e). Some of the bivalve shells were dissolved, leaving either moldic pores or pores filled with clear drusy calcite spar (Fig. 5a). Fibrous cements are found around the allochems or in intraparticle pores (Fig. 6a and b). Packstones occur in both the inner bank facies and the outer bank facies (Wu et al. 2019).

Wackestones

Wackestone is composed of foraminifera, calcareous algae, coralline crusts, bryozoans and small mollusc fragments, which are similar to the components of the packstone. The grains make up 15–60% of the whole rock with moderate to poor sorting and sub-rounded to sub-angular (Fig. 3f). Wackestones also occur in both the inner bank facies and the outer bank facies (Wu et al. 2019).

Diagenetic features

The reef-carbonate rocks show evidence of diagenetic effects such as dissolution, cementation, micritization and neomorphism (Fig. 8). Well-developed dissolution features are noticed in these reefal carbonates, especially at 0–180 m. A

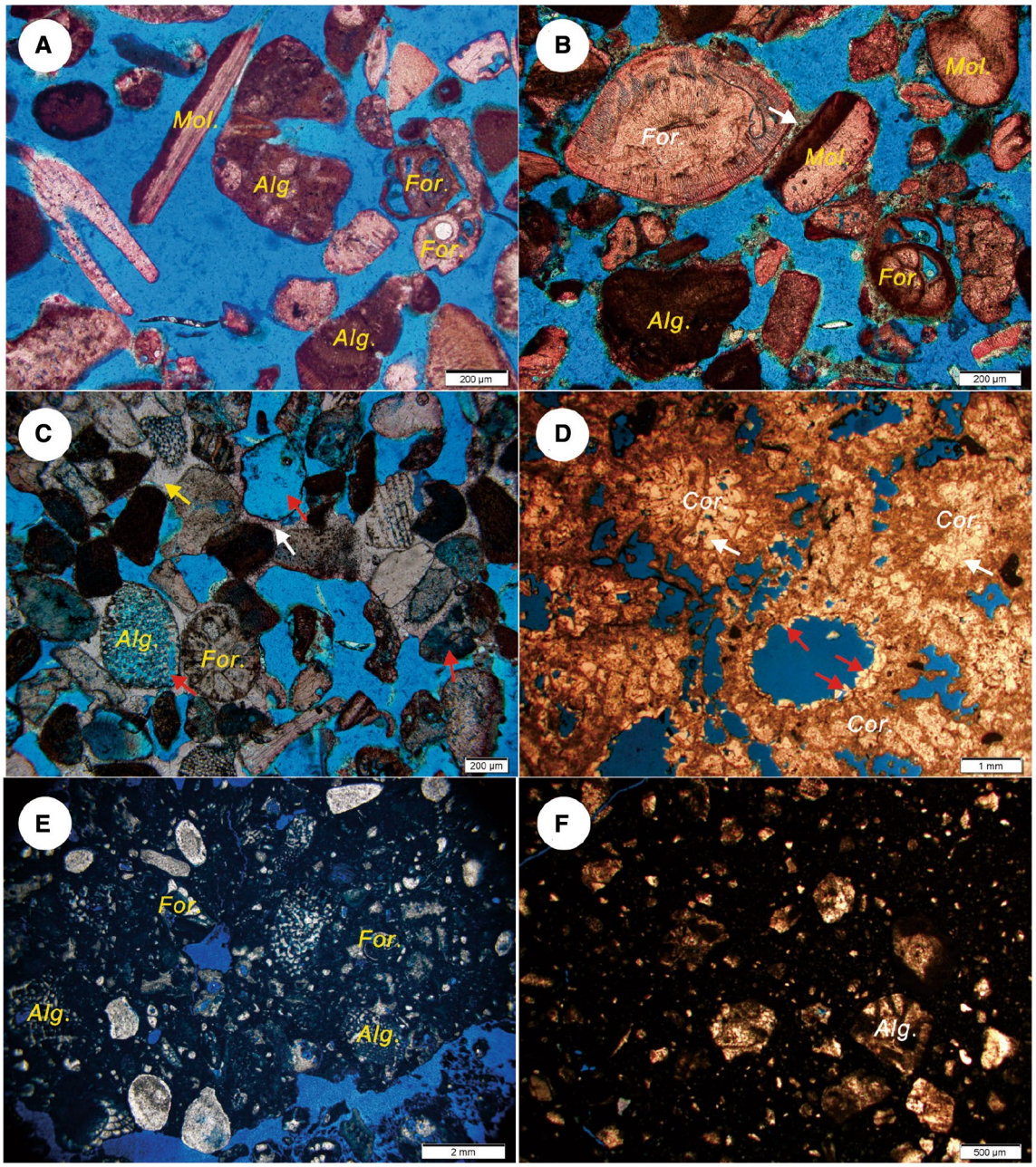

Fig. 3 Main reef-carbonate rock types in the Ledong formation, Pleistocene–Holocene. All images are in plane polarized light; blue = porosity. **a** Unconsolidated carbonate sands, with rare cement or matrix, 0.03 m. **b** Unconsolidated carbonate sands, part of grains connected with meniscus calcite cements (white arrow), 12.46 m. **c** Grainstone with partly or entire dissolved biodetritus (red arrows). Cements are meniscus (white arrow) or drusy calcite spar (yellow arrow), 7.61 m. **d** Framestone with pores within the corals partly filled with dogtooth (red arrow) and drusy calcite cements (white arrow), 137.57 m. **e** Packstone, the biodetritus made up 65% of the whole rock, 110.42 m. **f** Wackestone, 155.53 m. *For* foraminifer, *Cor* corals, *Alg* algae, *Mol* molluscs

large number of original bioclasts, such as mollusc shells, coral fragments and red algaes have been partly dissolved (Figs. 4a–c and 6c). Some bivalve shells have been completely dissolved, leaving molds defined by calcite cements (Fig. 4a and f). Dissolution also occurred on some early generated isopachous fibrous cements (Fig. 5e). Micritization of grains is relatively weak, but where present, a micrite envelope coats grains and lines cavities 2–10 µm in diameter. This envelope defines shell outlines after the shells have been dissolved away (Fig. 4a).

The term 'neomorphism' is used to include all transformations of minerals to polymorphs or crystalline structures that are structurally identical to the original material (Tucker 2001). The original aragonitic and high-Mg calcite biofragments, including red algae, coral skeleton and mollusc shells, have been altered or recrystallized to low-Mg calcite fragments (Figs. 4h and 5g).

Cements are extensively developed in these reefal carbonates. There is a wide variety of cement morphologies and the mineralogy is ether aragonite or calcite. The cement that occupies the majority of the original pore space is drusy calcite spar. These drusy calcite spar cements, which are mostly developed in 10.88–180 m, normally grow in the intragranular pores and are characterized by an increasing crystal size away from the substrate towards the cavity center (Figs. 4g, and 5c). The meniscus (Fig. 4c and e) and pendant (Fig. 4d) cements are present at depths shallower than 67 m, especially at 0–7.74 m. Isopachous dogtooth cements (Figs. 4b, 5a and b) first appear at depth of 7.74 m, and mainly developed at depth shallower than 180 m. Isopachous fibrous cements (Fig. 6a and b), normally fringing intraparticle pores of packstones are widespread at depths from 180 to 216 m. Sometimes, two generations of cements can be observed at depths shallower than 180 m, showing the grains was cemented by early isopachous fibrous calcite cements, and followed by drusy calcite spar cements (Fig. 5d and f). Most of the cements show non-luminescent character (Fig. 7b and h), occasionally with a thin (< 100 μm) brightly luminescent rim, whereas bioclasts generally show dull to bright luminescence (Fig. 7d and f).

C and O isotopic data

The $\delta^{18}O$ values (VPDB) for the carbonate rocks range between −8.4 and 1.5‰, with corresponding $\delta^{13}C$ values (VPDB) between −5.3 and 1.5‰ (Fig. 8). The bulk-rock stable isotope data for the upper 216 m of the cored succession can be divided into three intervals with gradational contacts: (1) an upper interval (depth) with negative values; (2) a transitional interval (depth) where the values gradually shift toward significantly negative values; and (3) a lower interval (depth) with relative high values. Significantly negative values are found from 22.96 to 169.62 m, where $\delta^{13}C$ values are between −5.3 and 0.2‰, with a mean of −2.4‰. Corresponding $\delta^{18}O$ values range from −8.4 to −4.6‰, with an average of −7.2‰ (Fig. 9, Table 1).

It would have been desirable to analyze the cements individually, but their small sizes precluded any systematic study. Regardless of this methodological limitation, the C and O isotopic data for the corals (Shao et al. 2017), which are selected from the bulk rock, closely mimic our bulk-rock data.

Discussion

Meteoric diagenesis

Lower limit of meteoric diagenesis

The upper part of the cored interval has been heavily altered by meteoric fluids. Unequivocal evidence of meteoric diagenesis includes consistently negative $\delta^{18}O$ values, well-developed subaerial exposure horizons and typical vadose cements. The transition from meteoric to marine diagenesis is best seen in the bulk-rock $\delta^{18}O$ data. The $\delta^{18}O$ values (VPDB) are −0.2‰ to −8.4‰ down to a depth of 169.62 m, where they begin a transition to more positive values, reaching a purely marine value of approximately +0.6‰ at 182 m. Thus, the base of meteoric diagenesis is defined as the deepest point with $\delta^{18}O < 0$, which is in the depth of ~ 180 m.

Five exposure horizons are distinguished (Fig. 2), which are likely the locations for the infiltration of meteoric water. Both the cement mineralogy and the nature of the cement fabrics provide evidence for meteoric diagenetic environment. The general patterns of the mineralogy are consistent with three intervals identified: a top interval of 0–21.66 m with low-Mg calcite and preserved aragonite and high-Mg calcite; a middle interval of 21.66–35.34 m with low-Mg calcite and preserved aragonite and a lower depth interval of low-Mg calcite (XRD data, Zhai et al. 2015). Under freshwater influence, high-Mg calcite cements can be converted to low-Mg calcite in a few thousand years, whereas calcitization of aragonite may take tens of thousand years (Gavish and Friedman 1969). Typical petrographic features related to the vadose zone are meniscus (Fig. 4c and e) and pendant calcite cements (Fig. 4d), dissolved pores (Fig. 4a, b and f) and the residual intergranular rounding pores (Fig. 4c), while the end products of phreatic meteoric diagenesis are the limestones composed of low-Mg calcite with micrite envelopes (Fig. 5a), moldic pores (Fig. 5a), blocky spar cements (Fig. 5c, d and g), and neomorphic bioclastics (Fig. 5g and h).

The grainstone (presenting at 3.22–10.88 m) records the boundary between the vadose and phreatic zones, which is marked by the first appearance of isopachous dogtooth cements (Fig. 4b). The meniscus textures seen from the depth shallower than 7.74 m indicate the presence of a meteoric vadose diagenetic zone (Longman 1980). It has been suggested that $\delta^{18}O$ values become heavier in the vadose zone, reflecting the loss of ^{16}O by evaporation (James and Choquette 1984). Carbonate sands in the uppermost 3.22 m of the core represent an exposed vadose soil horizon. From 2.92 to 7.74 m, calcite cements are

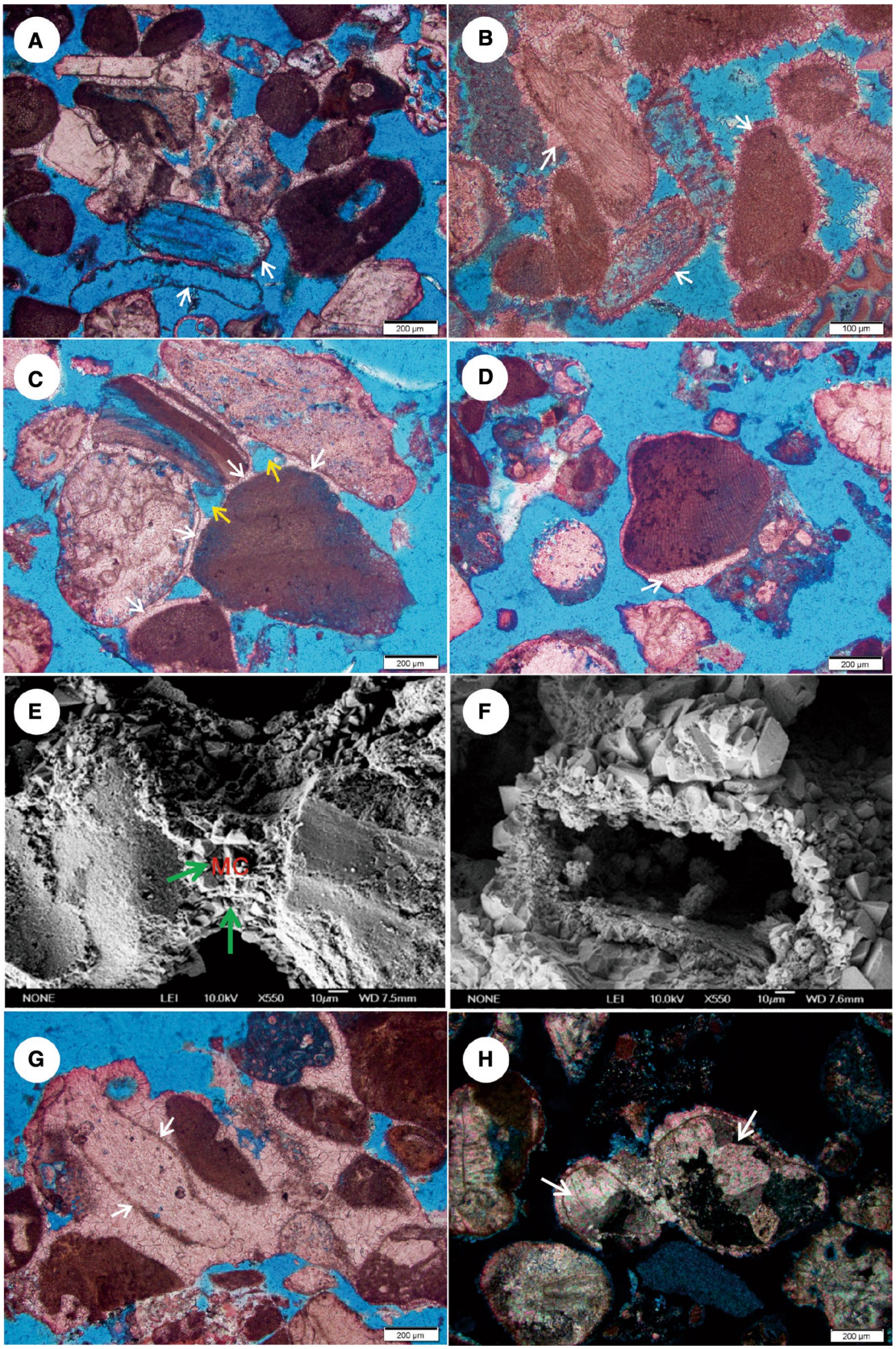
A
200 µm
B
100 µm
C
200 µm
D
200 µm
E
MC
NONE LEI 10.0kV X550 10µm WD 7.5mm
F
NONE LEI 10.0kV X550 10µm WD 7.6mm
G
200 µm
H
200 µm

◂**Fig. 4** Photomicrographs of products of meteoric diagenesis. **a**–**d** and **g** are taken under plane polarized light, **e** and **f** are from SEM, **h** is taken under cross-polarized light, blue = porosity. **a** Dissolved bioclasts, leaving molds with micrite envelopes (white arrows). Note some thin early calcite rims around some grains, 6.67 m, meteoric vadose zone. **b** Isopachous dogtooth calcite cements (white arrows), surrounding bioclasts. Some of the original bioclasts have been dissolved, 7.96 m, stained thin section, meteoric–phreatic zone. **c** Grains are connected by meniscus calcite cements (white arrows) causing rounded pores (yellow arrows), 6.2 m, meteoric vadose zone. **d** Pendant calcite cements (white arrow), 3.52 m, meteoric vadose zone. **e** Grains are connected by meniscus calcite cements (green arrows), 7.24 m, meteoric vadose zone. **f** Bioclasts have been dissolved, leaving molds defined by calcite cements, 7.96 m, meteoric–phreatic zone. **g** Drusy calcite spar, characterized by an increasing crystal size away from the substrate towards the cavity center. Note the calcite rims (white arrows) before the drusy calcite, 10.88 m, meteoric–phreatic zone. **h** Neomorphism occurred on red algae (white arrows), 10.88 m, meteoric–phreatic zone. *ME* meniscus cements

present as meniscus and pendant, with non-luminescent CL character (Fig. 7b), which are typical of vadose meteoric environments. From 7.74 to 10.88 m, the presence of abundant clear pore-filling isopachous dogtooth calcite cements (Fig. 5b) and moldic pores (Fig. 5f) suggest a phreatic environment. Therefore, the boundary between the vadose and phreatic zones might be 7.74 m. Similar features have been reported in oolitic limestone in Holocene strata from the Bahamas (Halley 1979; Budd 1988).

The framestones, packstones and wackestones between 21.66 and 180 m depth appear to have favored meteoric–phreatic diagenesis. The diagenesis in this interval produced limestones composed of low-Mg calcite with moldic pores (Fig. 5a) and drusy (Fig. 5c, d and g) or dogtooth calcite cements (Fig. 5a and b). Most of the cements show non-luminescent CL character (Fig. 7d), however, some brightly luminescent patches are present due to neomorphism (Fig. 7f).

Comparable studies in Xichen#1, located in the Yongle Atoll of the Xisha Islands (Fig. 1a), have produced strikingly similar petrographic and isotopic distribution patterns for Pleistocene–Holocene reef deposits (Fig. 9) (Liu et al. 1997, 1998). In Xichen#1, $\delta^{13}C$ and $\delta^{18}O$ values decrease rapidly from depths of 10–27 m, and become significantly negative from 27 to 165 m. Thus, the sections of 0–165 m have experienced meteoric diagenesis, which is similar to Xike#1. In addition, a mixing zone in the Early Pleistocene interval (165–179 m) was deduced with the systematic change from negative to positive $\delta^{13}C$ and $\delta^{18}O$ values with increasing depth. However, the co-variation between $\delta^{13}C$ and $\delta^{18}O$ values is not an unequivocal indicator of the mixing zone diagenesis. Swart and Oehlert (2018) propose that the co-varying trend is a consequence of varying degrees of alteration, rather than the result of diagenesis occurring within the zone where marine and freshwater fluids mix. Hence, we propose that the lower limit of meteoric diagenesis is about 180 m.

Because the recovery rate of Xike#1 is as high as nearly 80%, all the exposure surfaces present within the interval have been recorded. Thus, the deepest exposure surface (97.58–98.84 m) is ~ 80 m above the base of meteoric diagenesis. Melim (1996) suggest a maximum distance of ~ 60 m between the base of a diagenetically active meteoric lens and the land surface in the Pliocene–Pleistocene of Florida and Great Bahama Bank. While in Xike#1, the diagenetically active meteoric lenses can be restricted to 80 m, which is much deeper. The likely reasons for the deeper active meteoric lenses might be (1) a rapid transit through thin vadose zone leaves it water undersaturated when it enters the lens, and (2) abundant organic matter from soil zone is transported to the lens.

The record of meteoric diagenesis event

A completely meteoric realm in the upper portion (0–21.66 m) and a combination of meteoric and marine realm (21.66–180 m) in the lower portion can be distinguished in the core at depth of 0–180 m.

The upper 21.66 m of the core has been defined as aeolianites and this formed during marine isotope stage 3 (ca 70–30 ka) (Li et al. 2018). Li et al. (2018) considered that the depth interval of 3.22–10.88 m has been supplied with a higher amount of meteoric water, with the fact that both $\delta^{18}O$ values and Sr concentrations in this unit display lower values. Thus, this interval experienced more diagenetic alteration than the aeolianites above and below.

The interval between 21.66 and 180 m should have experienced multi-diagenesis during the successive Pleistocene sea-level variations. The framestones in this interval recorded a transferable diagenetic environment from marine to meteoric. The early-stage marine cements in reef structures are fibrous and acicular, most of which are surrounded by drusy morphologies, showing multiple generations of cementation (Fig. 5d and f). The development of drusy calcite cements on top of the marine cements suggests a later meteoric diagenesis. Some of the marine fibrous cements have elongate, intracrystalline cavities and voids along the cement layer as a result of meteoric dissolution (Fig. 5d), while some early-stage fibrous cements have been directly dissolved (Fig. 5e). Similar observations of the two generations of cementation were made by Vollbrecht (1990); Vollbrecht and Meischner (1996) in Pleistocene rocks on Bermuda. As mentioned earlier, there is a maximum distance of ~ 80 m between the base of the diagenetically active meteoric lens and the oldest paleoexposure surface, and considering the location of these five exposure horizons, there should be repeated meteoric infiltration occurred in these reef-carbonate rocks. Some meniscus cements can be

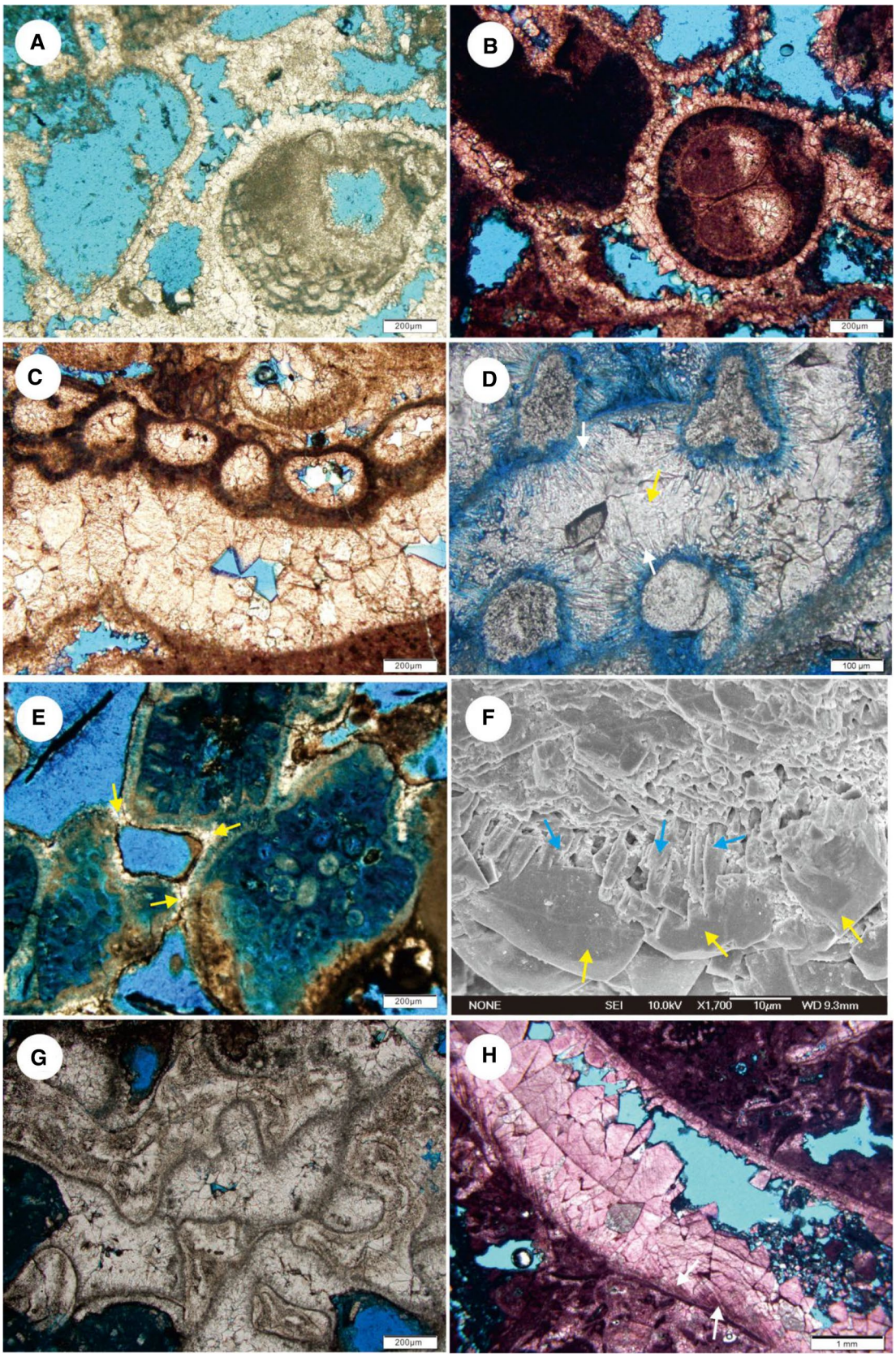
A
200µm
B
200µm
C
200µm
D
100 µm
E
200µm
F
NONE SEI 10.0kV X1,700 10µm WD 9.3mm
G
200µm
H
1 mm

◂**Fig. 5** Photomicrographs of products of meteoric diagenesis. **a**–**e** and **g** to **h** are taken under plane polarized light, **f** is from SEM, blue = porosity. **a** Isopachous dogtooth fringe around grains, 162.19 m, meteoric–phreatic zone. **b** Dogtooth cements, forming isopachous fringes, 160.72 m, stained thin section, meteoric–phreatic zone. **c** Drusy calcite spar growing in the intragranular pores, 157.53 m, meteoric–phreatic zone. **d** Two generations of cements, the grains cemented by early isopachous fibrous calcite cements (white arrows), followed by drusy calcite spar cements (yellow arrow), 27.08 m, meteoric–phreatic zone. **e** Early isopachous fibrous marine cements dissolved (yellow arrows), the grains are connected by meniscus cements (yellow arrows), 27.54 m, meteoric–phreatic zone. **f** Two generations of cements. Grains cemented by early isopachous fibrous calcite cements (blue arrows), then followed by drusy calcite spar cements (yellow arrows), 27.94 m, meteoric–phreatic zone. **g** Neomorphosed coral skeleton with internal sediment and/or calcite cements in skeletal voids, it is unclear if drusy calcite and neomorphism occurred in the same time, 27.08 m, meteoric–phreatic zone. **h** Part of molluscs shows neomorphism with relics of ultrastructure of the bioclasts (white arrows), whereas the other partially is dissolved and filled with a clearer calcite cement, 165.65 m, meteoric–phreatic zone

found with the depth of 27.54 m (Fig. 5e), which indicated an ancient vadose zone, related to the secondary exposure surface from the top of the interval. However, the diagenetic records of repeated sea-level changes are rare and most of them lack multiple cement generations. The meteoric–phreatic zone is much more active than the meteoric vadose zone (Steinen and Matthews 1973). During the sea-level changes, the water table moves through the sediments, thus the earlier diagenetic signatures have been finally destroyed and overprinted by the pervasive meteoric diagenesis (Vollbrecht and Meischner 1996; Gischler et al. 2013).

Marine diagenesis

From a depth of ~ 180 m to the base of Pleistocene strata, the most prevalent carbonate cements are fibrous, mostly appearing as isopachous fringes around grains (Fig. 6a and b). It is now generally accepted that most fibrous calcite cements are primarily marine precipitates (Tucker et al. 2008). The $\delta^{13}C$ values (PDB) range from − 1.4 to 0.4‰, with a mean of 0.7‰, and the $\delta^{18}O$ values (PDB) range from + 0.6 to + 1.5‰, which are expected in a marine diagenetic environment (Gonzalez and Lohnmann 1985). The cements'

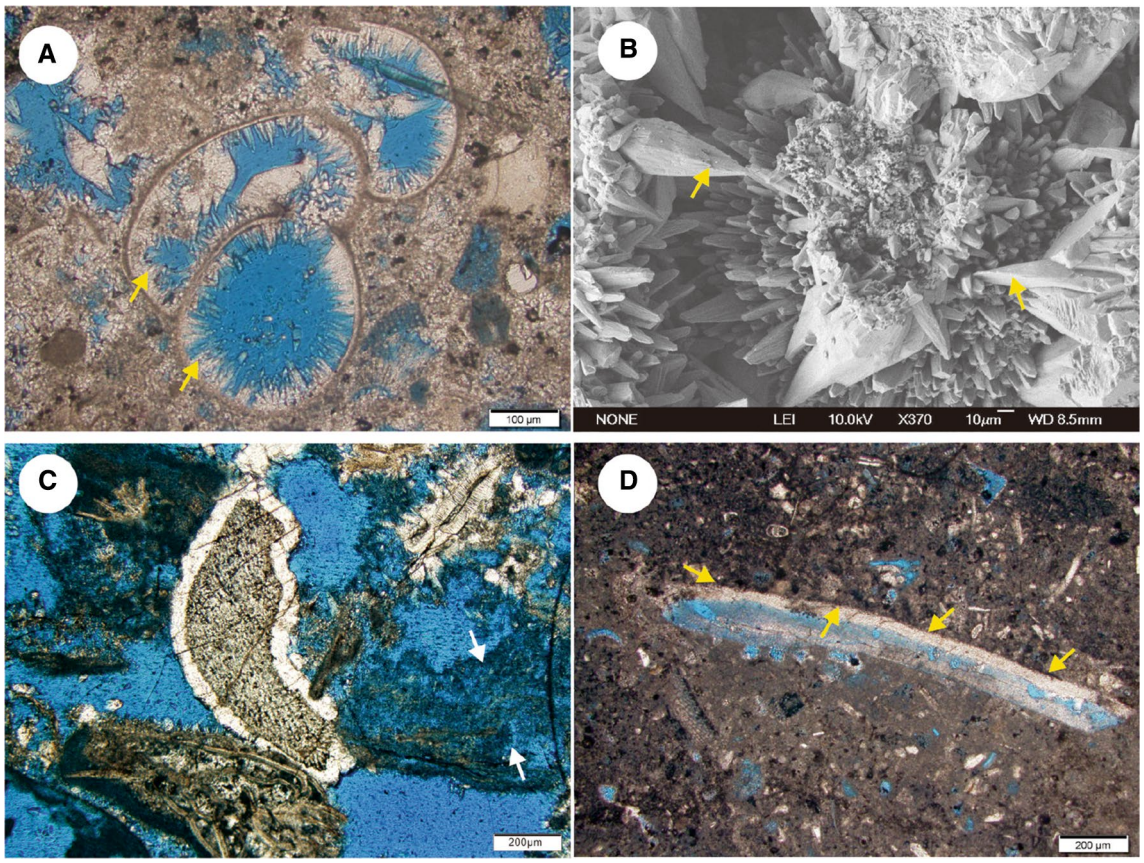

Fig. 6 Photomicrographs of products of marine diagenesis. **a**, **c** and **d** are taken under plane polarized light, **b** is from SEM, blue = porosity. **a** Isopachous fibrous calcite fringe in intraparticle pores (yellow arrows), 211.93 m. **b** Good preservation of well-developed fibrous calcite cements (yellow arrows), 212.6 m. **c** Syntaxial overgrowth on echinoderm fragment, note the dissolution for part of the red algae (white arrows), 211.93 m. **d** Micritization developed around the bioclasts (yellow arrows), 215.39 m

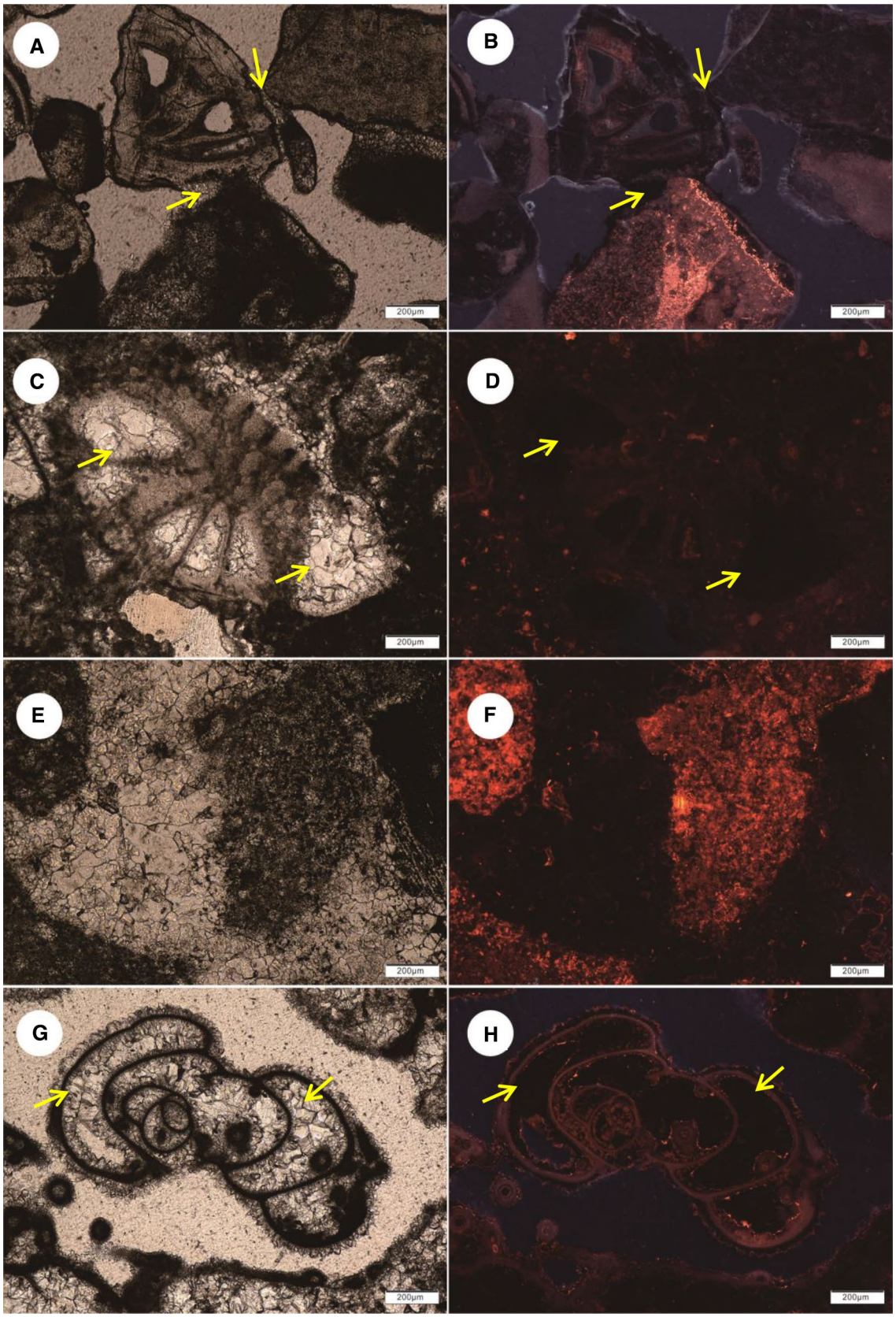
A
B
C
D
E
F
G
H
200μm

◂**Fig. 7** Photomicrographs of diagenetic cements with cathodoluminescence characteristic. **a**, **c**, **e** and **g** are taken under plane polarized light, while **b**, **d**, **f** and **h** are taken under cathodoluminescence. **a**, **b** Grains are connected by meniscus calcite cements (yellow arrows), which shows non-luminescent characteristic, 3.15 m, meteoric vadose zone. **c**, **d** Drusy calcite spar cements in intraparticle pores of foraminifera showing non-luminescent CL characteristic (yellow arrows), 27.94 m, meteoric–phreatic zone. **e**, **f** Drusy calcite spar showing non-luminescent CL with a thin (< 100 μm) brightly luminescent rim, whereas bioclasts generally show dull to bright luminescence, 169.62 m, meteoric–phreatic zone. **g**, **h** Isopachous fibrous fringe in intraparticle pores of foraminifera showing non-luminescent CL characteristic (yellow arrows), 211.93 m, marine diagenesis

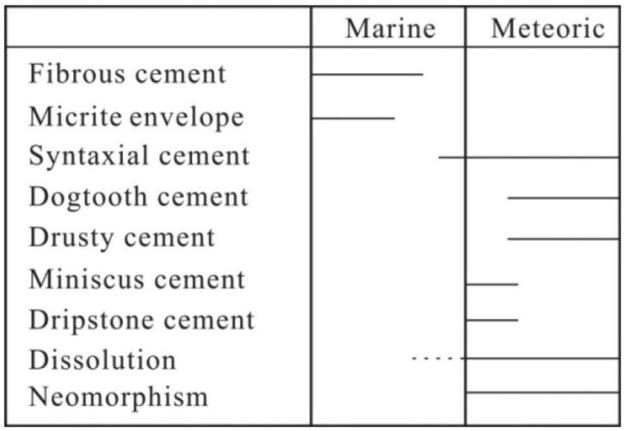

Fig. 8 Possible temporal sequence of diagenetic features observed in Xike#1

geometries, with a non-luminescent appearance (Fig. 7g and h), combined with limited, relatively enriched C and O isotope compositions, are suggestive of a marine diagenetic environment without any influence of meteoric water.

In low-latitude, shallow marine environments, marine fibrous cements typically precipitate in active marine diagenetic environments, with a more active pore fluid, while the grain micritization is indicative of low-energy conditions (Tucker et al. 2008). In Xike#1, the marine diagenetic products are varied in response to the different rock types. The packstones are characterized by a more widespread cementation (Figs. 4b and 6a), while the wackestones have ubiquitous microbial micritization (Fig. 6d), but limited cementation. Thus, a variable marine sedimentation environment can be deduced.

Rare syntaxial overgrowth cementation (Fig. 6c) and dissolution (Fig. 6c) also occurred in packstones with evidence of deposition in a high-current activity. The aragonite skeletons and aragonite/high-Mg calcite cements have been almost completely transformed to calcite (Fig. 9).

Responses to sea-level fluctuation and the sedimentation rate

The sea-level fluctuations and the rate of sedimentation were two important factors controlling the diagenesis of the strata. The exposure horizons in Xike#1 are more frequent

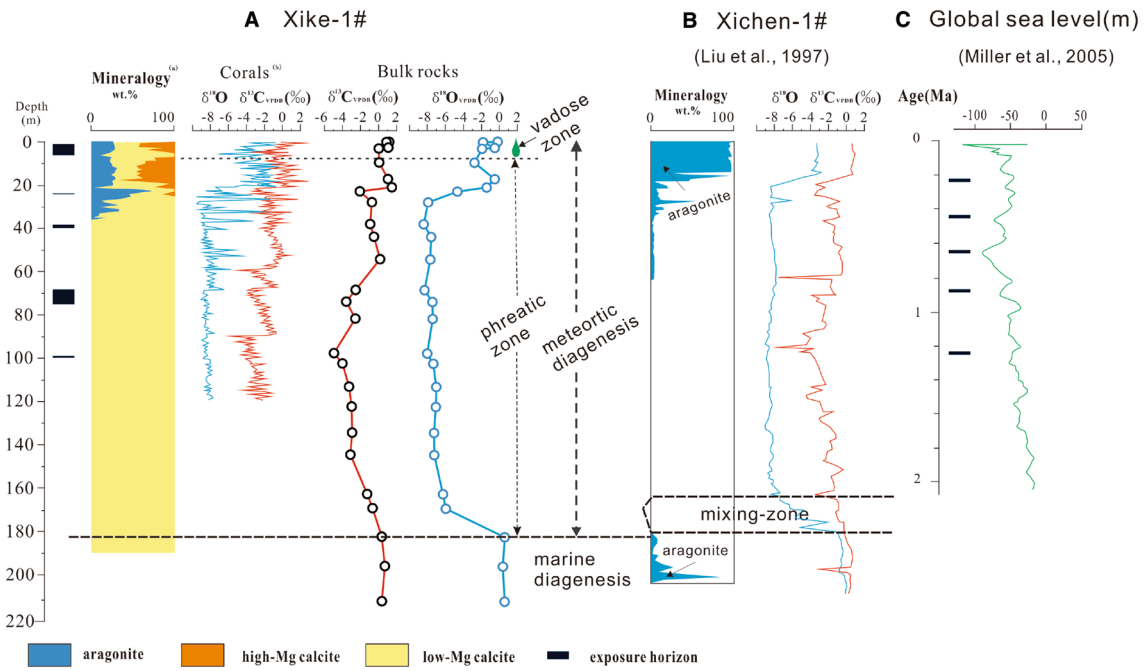

Fig. 9 **a** Distribution of diagenetic environments and the oxygen and carbon isotope values from 0 to 216 m of the Xike#1. **a** The mineralogy data of Xike#1 is from Zhai et al. (2015) by bulk X-ray analysis, the percentage of aragonite is shown from left to right and percent of high-Mg calcite is from right to left; **b** stable C and O isotopic data for the selected corals of Xike#1 is according to Shao et al. (2017); **b** the mineralogy and isotopic data in Xichen#1 (Liu et al. 1997); **c** Eustatic sea-level changes in the Pleistocene–Holocene (Miller et al. 2005)

Table 1 Carbon and oxygen isotope composition from reef carbonate in Ledong Formation, Quaternary of Xike-1 well

Depth	$\delta^{13}C_{V\text{-}PDB}$ ‰	$\delta^{18}O_{V\text{-}PDB}$ ‰	Remark
0.08	1.2	−0.2	a
0.2	0.9	−1.8	b
2.75	1.1	−0.5	a
3.15	0.1	−1.9	a
7	0.5	−3.5	a
9.6	0.1	−2.8	a
10.4	−0.4	− 2.4	a
17.26	1.1	−0.5	a
21.06	1.5	−1.4	b
21.96	−3.1	−3.9	a
22.96	−2.0	−4.6	a
24.06	−2.0	−5.0	a
27.94	−0.7	−7.9	a
36.32	−1.1	−7.8	a
37.5	−0.5	−7.6	a
38.25	−0.9	−8.4	b
44.11	−0.5	−7.6	a
51.28	−0.1	−7.4	a
54.47	0.2	−7.6	a
66.69	−1.9	−7.2	a
68.67	−2.5	−8.3	b
71.47	−0.7	−7.3	a
74.12	−3.5	−7.4	a
74.3	−3.3	−7.6	a
78.48	−2.8	−7.4	a
82	−2.5	−7.4	a
97.97	−4.9	−8	b
98.53	−3.5	−7.3	a
100.08	−5.3	−7.2	a
102.7	−4.0	−7.3	a
109.77	−3.8	−6.9	a
113.44	−3.2	−7.0	a
117.59	−3.3	−7.4	b
122.62	−2.9	−7.0	a
124.04	−2.8	−6.8	a
130	−4.1	−7.1	a
134.7	−2.9	−7.2	a
144.88	−3.1	−7.2	a
163	−1.2	−6.2	a
169.62	−0.6	−5.9	a
182.83	0.4	0.6	a
186.7	0.6	−0.3	a
196.4	0.7	0.4	a
212.6	0.4	0.6	a
216	1.4	1.5	a

Remark: *a* analyzed in the Institute of Geology Chinese Academy of Geological Sciences, *b* analyzed in the CNNC Beijing Research Institute of Uranium Geology, China

after 1.25 Ma. The ages of these exposure horizons can be correlated with the timing of eustatic falls in global sea-level change derived from oxygen isotopic data (Miller et al. 2005) (Fig. 9c). The top of the meteoric lens closely follows sea level, and accompanied by the oscillation of sea level, the water table could move through the sediments. Thus, the upper part of the cored interval (0–180 m) was heavily altered by meteoric fluids.

Sedimentation rate variations could also be another important potential factor controlling the diagenetic evolution. The sedimentation rate transition can be divided into four stages according to the age–depth model established by Wang et al. (2017), which are: (1) 1.78–2.0 Ma, 50 m/Ma (2) 1.1–1.78 Ma, 290–160 m/Ma; (3) 0.15–1.1 Ma, 24–72 m/Ma; (4) 0–0.15 Ma, 217 m/Ma (Fig. 10). Diagenesis tends to be active and complete in a lower sedimentation rate, as seawater had a long time to make a contact with the sediments. Thus, cements will be better developed in areas of slow sediment accumulation or slow reef growth. It is interesting that the base of meteoric diagenesis at ~ 180 m is roughly paralleled by an abrupt increase in the sedimentation rate at ~ 1.78 Ma. During 1.1–1.78 Ma, the growth of the cements might be influenced by the relative high-sedimentation rate, resulting in the meteoric water being potentially saturated with regard to calcium carbonate before reaching a deep lens. Thus, the diagenetically active meteoric lenses in Xike#1 can be extended to 80 m below the exposure horizon, which is 20 m deeper than that in Bahamas (Melim 1996). This increase in the sedimentation rate start at ~ 1.78 Ma was controlled jointly by regional subsidence (Wang et al. 2017) and nutrient variations (Wu et al. 2019). As the nutrient excess can hinder coral growth (Hallock and Schlager 1986), Wu et al. (2019) found that the abrupt increase in coral abundance and the occurrence of reef facies was most probably caused by the rapid nutrient decrease. The second turnover of the sedimentation rate occurred at 1.1 Ma. The sedimentary rate is relatively slow at 0.15–1.1 Ma, while the decline in general sedimentation rate could be derived from non-deposition and erosion events during the exposure periods. With these erosion events, repeated meteoric infiltration with multi-stage cementation and dissolution could occur. However, a relatively more active diagenesis in the slower sedimentary rate might finally destroy and overprint the earlier diagenetic signatures, leading to diagenetic records of repeated sea-level changes not being preserved. The third turnover of the sedimentation rate occurred at 0.15 Ma, which was accompanied by the formation of the aeolianites. Most of the aeolianites are present as weak cementation and the inadequate diagenesis is probably due to the increase in sedimentation rate.

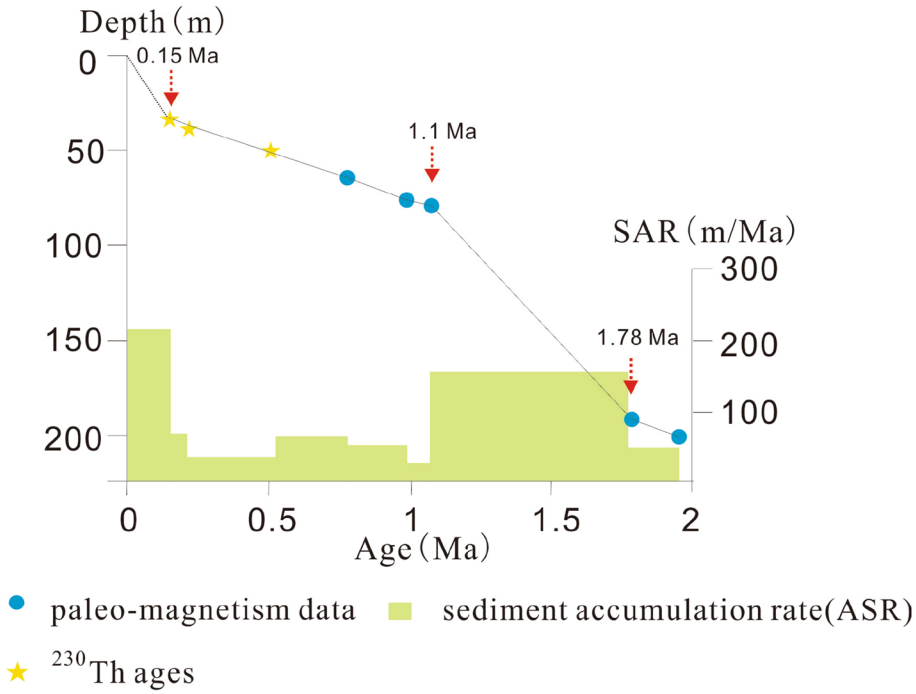

Fig. 10 Age–depth chart and the sediment accumulation rate for Xike#1 (according to Wang et al. 2017)

Diagenetic evolution

The Pleistocene–Holocene reef-carbonate rocks in Xike#1 penetrate trough the zone of meteoric diagenesis into an underlying interval where only marine diagenesis is evident.

Only marine diagenesis occurred in the interval between 180 and 216 m. The diagenetic products are related to the marine sedimentation environment: (1) within the high-energy shallow marine environment, fibrous cements are produced which vertically grow on the biodetritus, syntaxial cements which are overgrown on echinoderms fragments, and partial dissolution of the red algae (Fig. 11b); (2) within the relatively stagnant shallow marine environment, the products are ubiquitous microbial micritization and partial dissolution of the red algae (Fig. 11c). However, it is usually difficult to determine whether micrite in these wackstones is indeed a marine cement or fine-grained marine sediment.

The other two kinds of diagenetic models are presented in Figs. 12 and 13 for the interval that was influenced solely by meteoric water in the upper portion (0–21.66 m) of the core and a combination of meteoric and marine realm in the lower portion (21.66–180 m), respectively.

In the interval of 0–21.66 m, the sediments are identified as aeolian carbonate sands, which were derived from a subtropical subtidal environment (Li et al. 2018). The formation of the aeolianite deposits was probably related to the intensified winter monsoon which provided a strong wind to blow skeletal grains onshore (Wu et al. 2019). Within the decline of sea level and the cooling event, for these original sediments, the initial effects of the diagenesis may be dissolution and cementation induced by meteoric water infiltration. Diagenetic features of vadose zone are characterized by: (1) widespread meniscus and pendant cements, (2) high-Mg calcite/aragonite grains are either converted to low-Mg calcite or dissolved out, leaving moldic pores lined by micrite envelopes, (3) biodetritus show neomorphism with the relics of internal structure (Fig. 12b). In the phreatic zone, pore-filling isopachous dogtooth calcite cements are well developed. The original aragonite grains are more likely to be calcitized in places. The biodetritus are replaced by coarser calcite cements (Fig. 12c).

The sediments between 21.66 and 180 m which are influenced by both freshwater and marine water are mainly composed of the reef facies. Thus, the typical starting sediments were coral skeletons. Within the initial marine environment, cements appear as isopachous fibrous fringes in intraparticle pores (Fig. 13b). As the sediments got exposed when the sea level fell and then experienced meteoric diagenesis, intense dissolution, neomorphism and the formation of drusy cements occurred (Fig. 13c). Part of the early fibrous cements was dissolved, while the other part was preserved and cemented by the later meteoric drusy cements. Skeletons seem to be much more susceptible to cementation than dissolution, which are preserved in many cases and are overgrown by low-Mg calcite. It is unclear if the cementation of drusy calcite and neomorphism occurred at the same time.

Our results thus explain the diagenetic evolution history for the Pleistocene–Holocene reef-carbonate rocks in Xike#1, which was influenced by the sea-level fluctuation and the rate of the sedimentation. This finding provides

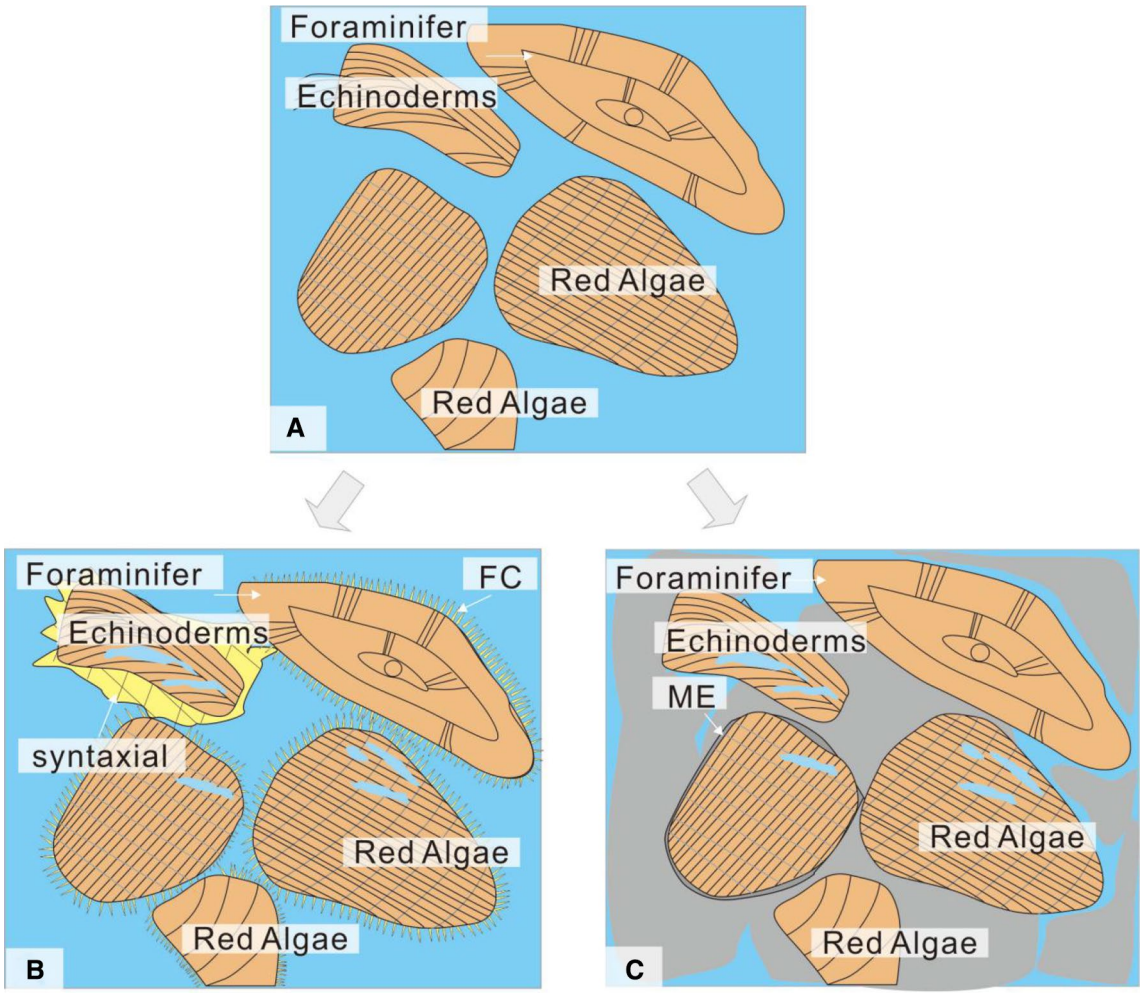

Fig. 11 Diagenetic evolution patterns in marine diagenesis. **a** Original grains with foraminifer, mollusc and red algae. **b** High-energy environment, the diagenetic products are characterized by aragonite fibrous cements, with rare syntaxial overgrowth on echinoderms and the dissolution of red algae. **c** In a more stagnant pore fluid, the diagenetic products are ubiquitous microbial micritization and partial dissolution of the red algae. *WP* intragranular pores, *FC* fibrous aragonite cements, *ME* micritization

petrographic, C and O isotope records for the diagenetic history of the tropical carbonate system in Xisha Islands, and further evidences the impact of high-frequency eustatic sea-level change on the diagenetic evolution of Xisha carbonate platform.

Conclusion

Detailed assessments of the mineralogical, petrographic and stable isotopic data from Xike#1 in Xisha Islands led to the following conclusion about the Pleistocene–Holocene reef-carbonate rocks.

The interval from 0 to 180 m has undergone meteoric diagenesis, with a completely meteoric realm in the upper portion (0–21.66 m) and a combination of meteoric and marine realm in the lower portion (21.66–180 m). The interval from 180 to 216 m has undergone a variation of marine diagenesis.

Meteoric diagenesis is marked by well-developed subaerial exposure horizons, vadose and phreatic cements with non-luminescent CL characteristics, and consistently negative C and O isotope values. The diagenetically active meteoric lenses can be extended to 80 m. Some of the samples recorded the two phases of both marine and meteoric diagenetic events, which show that the grains was cemented by early isopachous fibrous marine cements, then followed by drusy calcite spar cements. A diagenetic record of repeated sea-level changes is rare.

Meteoric diagenesis is characterized by limited, relatively enriched C and O isotope compositions, fibrous cements with non-luminescent CL characteristics and ubiquitous microbial micritization.

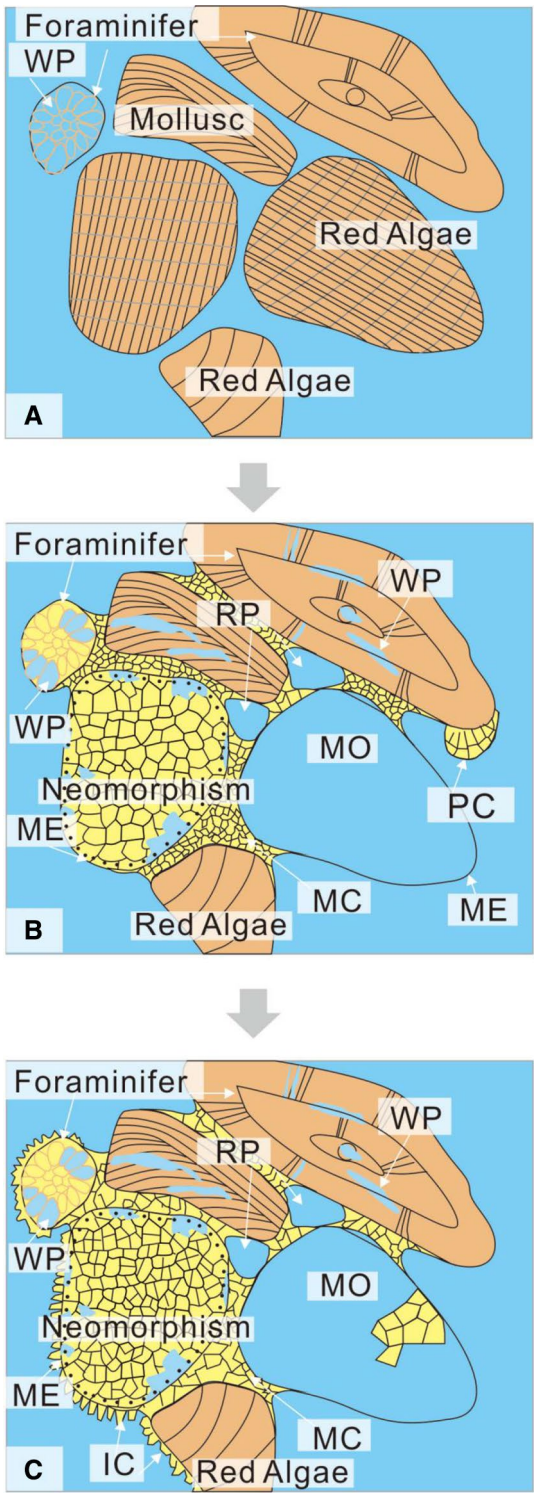

Fig. 12 Diagenetic products for grainstone in meteoric diagenesis (the depth of 0–21.66 m). **a** Original grains as unconsolidated carbonate sands. **b** End products, vadose zone. The calcite cements are present as meniscus and pendant textures, note the abundant moldic porosity and coeval with aragonite neomorphism. **c** End products, phreatic zone. Note the minor dogtooth spar cementation. *WP* intragranular pores, *RP* rounding pores, *MO* Moldic pores, *ME* micritization, *MC* meniscus cements, *PC* pendant cements, *IC* isopachous dogtooth fringe

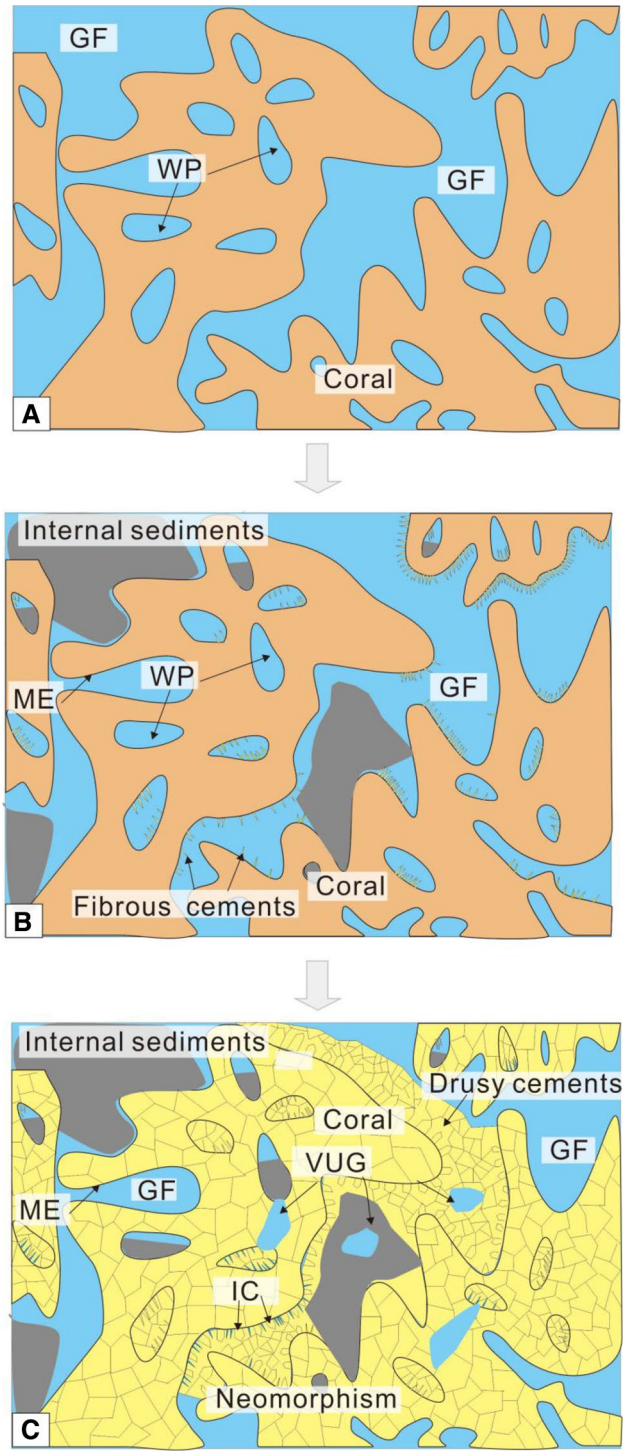

Fig. 13 Diagenetic products for framestone (21.66–180 m), controlled by the combination of marine and meteoric and marine diagenesis. **a** Original coral framework. **b** Fibrous aragonite cements with internal sediments infilling the framework and intergranular pores in early marine diagenetic environment. **c** Reef framework shows neomorphism with dogtooth or drusy calcite in the later meteoric diagenetic environment. Part of the early marine fibrous cements is preserved although dissolution is effective. It is unclear if the drusy calcite cements cementation and neomorphism occurred at the same time. *WP* intragranular pores, *GF* framework pores, *ME* micritization, *IC* isopachous dogtooth cements

The diagenetic evolution was shaped by both the eustatic sea-level fluctuation and sedimentation rate variations.

Acknowledgements This research was supported by National Major Scientific and Technological Special Project during the Twelfth 5-year Plan Period (no. 2011ZX05025-002), Major Subject of The CNOOC (CNOOC-2013-ZJ-01) and the National Natural Science Foundation of China (no. 41202073). Stable isotope analysis was performed in the Institute of Geology and Geophysics, Chinese Academy of Sciences, and in Analytical Laboratory Beijing Research Institute of Uranium Geology.

References

Allan JR, Matthews RK (1977) Carbon and oxygen isotopes as diagenetic and stratigraphic tools: surface and subsurface data, Barbados, West Indies. Geology 5:16–20

Allan JR, Matthews RK (1982) Isotope signatures associated with early meteoric diagenesis. Sedimentology 29:797–817

Benito MI, Mas R (2006) Sedimentary evolution of the Torrecilla Reef Complex in response to tectonically forced regression (Early Kimmeridgian, Northern Spain). Sediment Geol 183:31–49

Buchbinder LG, Friedman GM (1980) Vadose, phreatic, and marine diagenesis of Pleistocene–Holocene carbonates in a borehole: mediterranean coast of Israel. J Sediment Res 50:395–408

Budd DA (1988) Aragonite-to-calcite transformation during freshwater diagenesis of carbonates. Geol Soc Am Bull 100:1260–1270

Budd DA, Land LS (1990) Geochemical imprint of meteoric diagenesis in Holocene ooid sands, Schooner Cays, Bahamas: correlation of calcite cement geochemistry with extant groundwaters. J Sediment Res 60:361–378

Chen M, Huang C, Pflaumann U, Waelbroeck C, Kucera M (2005) Estimating glacial western Pacific sea-surface temperature: methodological overview and data compilation of surface sediment planktic foraminifer faunas. Quat Sci Rev 24:1049–1062

Dunham RJ (1962) Classification of carbonate rocks according to depositional texture. Memoir Am Ass Pet Geol 1:108–121

Embry A, Klovan JE (1971) A late Devonian reef tract on northeastern Banks Island, northwest territories. Bull Can Pet Geol 19:730–781

Follows EJ (1992) Patterns of reef sedimentation and diagenesis in the Miocene of Cyprus. Sediment Geol 79:225–253

Fox DL, Honey JG, Martin RA, Pelaez-Campomanes P (2012) Pedogenic carbonate stable isotope record of environmental change during the Neogene in the southern Great Plains, southwest Kansas, USA: oxygen isotopes and paleoclimate during the evolution of C^4-dominated grasslands. Geol Soc Am Bull 124:431–443

Gavish E, Friedman GM (1969) Progressive diagenesis in Quaternary to Late Tertiary carbonate sediments: sequence and time scale. J Sediment Petrol 39:980–1006

Gischler E, Thomas AL, Droxler AW, Webster JM, Yokoyama Y, Schne BR (2013) Microfacies and diagenesis of older Pleistocene (pre-last glacial maximum) reef deposits, Great Barrier Reef, Australia (IODP Expedition 325): a quantitative approach. Sedimentology 60:1432–1466

Gonzalez LA, Lohnmann KC (1985) Carbon and oxygen isotopic composition in Holocene reefal carbonates. Geology 13:811–814

Halley RB (1979) Freshwater cementation of a 1000-year-old oolite. J Sediment Petrol 49:969–988

Hallock P, Schlager W (1986) Nutrient excess and the demise of coral reefs and carbonate platforms. Palaios 1:389–398

He QX, Zhang MS (1990) Origin of Neogene dolomites in Xisha Islands and their significance. Mar Geol Quat Geol 10:45–55 **(in Chinese with English abstract)**

Huang C, Wu S, Zhao M, Chen M, Wang C, Tu X, Yuan PB (1997) Surface ocean and monsoon climate variability in the South China Sea since the last glaciation. Mar Micropaleontol 32:71–94

James NO, Choquette PW (1984) Diagenesis 9: limestones- the meteoric diagenetic environment. Geosci Can 11:161–194

Kindler P, Mazzolini D (2001) Sedimentology and petrography of dredged carbonate sands from stocking Island (Bahamas): implications for meteoric diagenesis and aeolianite formation. Palaeogeogr Palaeoclimatol Palaecol 175:369–379

Kumar SK, Chandrasekar N, Seralathan P, Sahayam JD (2012) Diagenesis of Holocene reef and associated beachrock of certain coral islands, Gulf of Mannar, India: implication on climate and sea level. J Earth Syst Sci 121:733–745

Lambeck K, Esat TM, Potter E-K (2002) Links between climate and sea levels for the past three million years. Nature 419:199–206

Li R, Jones B (2013a) Temporal and spatial variations in the diagenetic fabrics and stable isotopes of Pleistocene corals from the Ironshore Formation of Grand Cayman, British West Indies. Sediment Geol 286–287:58–72

Li R, Jones B (2013b) Heterogeneous diagenetic patterns in the Pleistocene Ironshore Formation of Grand Cayman, British West Indies. Sediment Geol 294:251–265

Li R, Qiao PJ, Cui YC, Zhang DJ, Liu XY, Shao L (2018) Composition and diagenesis of Pleistocene aeolianites at Shidao, Xisha Islands: implications for palaeoceanography and palaeoclimate during the last glacial period. Palaeogeogr Palaeoclimatol Palaeoecol 490:604–616

Lincoln JM, Schlanger SO (1987) Miocene sea-level falls related to the geologic history of Midway Atoll. Geology 15:454–457

Liu J, Ye ZZ, Han CR, Liu XB, Qu GS (1997) Meteoric diagenesis in Pleistocene reef limestones of Xisha Islands, China. J Asian Earth Sci 15:465–476

Liu J, Han CR, Wu JZ, Ju LJ (1998) Geochemical evidence for the meteoric diagenesis in Pleistocene reef limestones of Xisha Islands. Acta Sedimentol Sin 16:71–77 **(in Chinese with English abstract)**

Longman MW (1980) Carbonate diagenetic textures from near surface diagenetic environment. Am Assoc Pet Geol Bull 64:461–487

Ma ZL, Li QY, Liu XY, Luo W, Zhang DJ, Zhu YH (2018) Palaeoenvironmental significance of Miocene larger benthic foraminifera from the Xisha Islands, South China Sea. Palaeoworld 27:145–157

Major RP, Matthews RK (1983) Isotopic composition of bank margin carbonates on Midway Atoll: amplitude constraint on post-early Miocene eustasy. Geology 11:335–338

Martindale RC, Bottjer DJ, Corsetti FA (2012) Platy coral patch reefs from eastern Panthalassa (Nevada, USA): unique reef construction in the Late Triassic. Palaeogeogr Palaeoclimatol Palaeoecol 313–314:41–58

McCrea JM (1950) On the isotopic chemistry of carbonates and a paleotemperature scale. J Chem Phys 18:849–857

Melim LA (1996) Limitations on lowstand meteoric diagenesis in the Pliocene-Pleistocene of Florida and Great Bahama Bank: implications for eustatic sea-level models. Geology 10:893–896

Melim LA, Swart PK, Eberli GP (2004) Mixzong-zone diagenesis in the subsurface of Florida and the Bahamas. J Sediment Res 74:904–913

Miller KG, Kominz MA, Browning JV, Wright JD, Mountain GS, Katz ME, Sugarman PJ, Cramer BS, Christie-Blick N, Pekar SF (2005) The Phanerozoic record of global sea-level change. Science 310:1293–1298

Pelejero C, Grimalt JO, Heilig S, Kienast M, Wang L (1999) High-resolution UK37 temperature reconstructions in the South China Sea over the past 220 kyr. Paleoceanography 14:224–231

Qiao PJ, Zhu WL, Shao L, Zhang DJ, Cheng XR, Song YM (2015) Carbonate stable isotope stratigraphy of well Xike-1, Xisha Islands. Earth Sci 40:725–732 **(in Chinese with English abstract)**

Quade J, Roe LJ (1999) The stable-isotope composition of early ground-water cements from sandstone in paleoecological reconstruction. J Sediment Res 69:667–674

Quinn TM (1991) Meteoric diagenesis of Plio-Pleistocene limestones at Enewetak Atoll. J Sediment Petrol 61:681–703

Saller AH, Moore CH (1989) Meteoric diagenesis, marine diagenesis, and microporosity in Pleistocene and Oligocene limestones, Enewetak Atoll, Marshall Islands. Sediment Geol 63:253–272

Shao L, Cui YC, Qiao PJ, Zhang DJ, Liu XY, Zhang CL (2017) Sea-level changes and carbonate platform evolution of the Xisha Islands (South China Sea) since the Early Miocene. Palaeogeogr Palaeoclimatol Palaeoecol 485:504–516

Singh S, Parkash B, Awasthi AK, Singh T (2012) Palaeoprecipitation record using O-isotope studies of the Himalayan Foreland Basin sediments, NW India. Palaeogeogr Palaeoclimatol Palaeoecol 331–332:39–49

Solihuddin T, Collins LB, Blakeway D, O'Leary MJ (2015) Holocene coral reef growth and sea level in a macrotidal, high turbidity setting: cockatoo Island, Kimberley Bioregion, northwest Australia. Mar Geol 359:50–60

Steinen RP, Matthews RK (1973) Phreatic vs. vadose diagenesis: stratigraphy and mineralogy of a cored borehole on Barbados, W.I. J Sediment Petrol 43:1012–1020

Swart PK, Oehlert AM (2018) Revised interpretations of stable C and O patterns in carbonate rocks resulting from meteoric diagenesis. Sediment Geol 364:14–23

Tucker ME (2001) Carbonate reservoirs: porosity evolution and diagenesis in sequence stratigraphic framework, vol 55. Elsevier, Amsterdam, p 444

Tucker ME, Wright VP, Dickson JAD (2008) Carbonate sedimentology. Blackwell Science Ltd, Hoboken

Vollbrecht R (1990) Marine and meteoric diagenesis of submarine Pleistocene carbonates from the Bermuda carbonate platform. Carbonates Evaporites 5:13–95

Vollbrecht R, Meischner D (1996) Diagenesis in coastal carbonates related to Pleistocene sea level, Bermuda platform. J Sediment Res 66:243–258

Waelbroeck C, Labeyrie L, Michel E, Duplessy JC, McManus JF, Lambek K, Balbon E, Labracherie M (2002) Sea-level and deep water temperature changes derived from benthic foraminifera isotopic records. Quat Sci Rev 21:295–305

Wang ZF, Zhang DJ, Liu X, You L, Luo W, Yi L, Tan L, Zhu Y, Qin H, Cheng H, Li Z, Xie Q, Che Z, Deng C, Zhu R (2017) Magnetostratigraphy and ^{230}Th dating of Pleistocene biogenic reefs in XK-1 borehole from Xisha Islands, South China Sea. Chin J Geophys 60:1027–1038 **(in Chinese with English abstract)**

Wang Z, Huang K, Zhang D, You L, Liu X, Luo W (2018) Maturation of Neogene dolomite from Xuande Atoll of Xisha archipelago, the South China Sea. Mar Pet Geol 92:51–64

Woodroffe CD, Webster JM (2014) Coral reefs and sea-level change. Mar Geol 352:248–267

Wu S, Yang Z, Wang D, Lü F, Lüdmann T, Fulthorpe C, Wang B (2014) Architecture, development and geological control of the Xisha carbonate platforms, northwestern South China Sea. Mar Geol 350:71–83

Wu F, Xie XN, Betzler C, Zhu WL, Zhu YH, Guo LY, Ma ZL, Bai HQ, Ma BJ (2019) The impact of eustatic sea-level fluctuations, temperature variations and nutrient-level changes since the Pliocene on tropical carbonate platform (Xisha Islands, South China Sea). Palaeogeogr Palaeoclimatol Palaeoecol 514:373–385

Yasukochi T, Kayanne H, Yamaguchi T, Yamano H (2014) Sedimentary facies and Holocene depositional processes of Laura Island, Majuro Atoll. Geomorphology 222:59–67

Ye YG, Wang XE, Diao SB (1987) A preliminary study on the reliability of radiocarbon age from Shidao Island of Xisha Archipelago. Mar Geol Quat Geol 7:121–130 **(in Chinese with English abstract)**

Ye YG, He J, Diao SB, Gao CJ, Du YJ (1990) 14C and ESR ages of eolian calcarenite from Shidao Island of Xisha Island. Mar Geol Quat Geol 10:103–110 **(in Chinese with English abstract)**

Ye YG, He J, Diao SB, Liu X, Gao J Du YJ (1991) ESR chronology of well Xi-Chen-1. In: Correlation of onshore and offshore quaternary in China. Science Press, Beijing, pp 224–233 **(in Chinese with English abstract)**

Zhai SK, Mi LJ, Shen X, Liu XY, Xiu C, Sun ZP, Cao JQ (2015) Mineral compositions and their environmental implications in reef of Shidao Island, Xisha. Earth Sci J China Univ Geol 40:597–602 **(in Chinese with English abstract)**

Zhang MS (1990) Quaternary reef stratigraphic division in Hole Xiyong-1. Mar Geol Quat Geol 10:57–64 **(in Chinese with English abstract)**

Zhang MS, He QX, Ye ZZ, Han C, Li H, Wu J, Ju L (1989) Sedimentological studies of Xisha Organic reef carbonates. Science Press, Beijing **(in Chinese with English abstract)**

Zhu Y, Liu X, Ma R, Luo W, Wang X, Xu S (2016) Early Miocene to Quaternary Calcareous Nanofossils from the biogenetic reef complexes and their significance of Well XK1, Xisha Islands, South China Sea. Acta Palaeontol Sin 55:85–92 **(in Chinese with English abstract)**